Materials Today Bio 31 (2025) 101582

Contents lists available at ScienceDirect

Materials Today Bio

journal homepage: www.journals.elsevier.com/materials-today-bio

PLGA/HA sustained-release system loaded with liraglutide for the treatment of diabetic periodontitis through inhibition of necroptosis

Yunqing Pang [a,b,1], Lingyuan Kong [a,b,1], Yuanyuan Li [a,b,1], Jiamin Li [a,b], Qianlong Ma [a,b], Jing Qiu [a,b], Jing Wang [a,b,*]

[a] School/Hospital of Stomatology, Lanzhou University, Lanzhou, Gansu, 730000, China
[b] Clinical Research Center for Oral Diseases, Lanzhou, Gansu, 730000, China

ARTICLE INFO

Keywords:
DP
LIRA
Sustained-release system
PLGA

ABSTRACT

Diabetes and periodontitis exhibit a bidirectional relationship, posing significant challenges for the treatment of periodontitis in patients with diabetes. Our previous studies showed that the hypoglycemic agent liraglutide (LIRA), together with glycemic control, had favorable therapeutic effects on diabetic periodontitis (DP), achieving a "two birds with one stone" effect. Therefore, exploration of the topical application of LIRA for treating DP is warranted. In this study, nanoparticles were loaded with LIRA using poly (lactic-co-glycolic acid) (PLGA), and their morphology, particle size, encapsulation efficiency, drug loading, and drug release profiles were characterized. These nanoparticles were further encapsulated with hyaluronic acid (HA) to form a LIRA@PLGA/HA sustained-release system. The cytotoxicity of LIRA@PLGA/HA was analyzed using CCK-8 assays, and its anti-inflammatory and osteogenic effects on periodontitis in diabetic rats were evaluated by histology, ELISA, and micro-CT analysis, while its influence on necroptosis-related factors was assessed using qRT-PCR and Western blotting. The results indicated that LIRA@PLGA (30000 Da) exhibited an encapsulation efficiency of 86.2 %, a drug loading capacity of 4.3 %, and a cumulative release of LIRA reaching approximately 60 % after 8 days, thereby meting the requirement for sustained release. Following 24 h of stimulation with various concentrations (0–20 mg/ml) of LIRA@PLGA/HA, the viability of human periodontal ligament cells (HPDLCs) remained above 85 %. Topical application for four weeks significantly inhibited the expression of the inflammatory factors TNF-α and IL-1β in gingival crevicular fluid and serum, reduced inflammatory cell infiltration in periodontal tissues, and attenuated alveolar bone resorption while improving alveolar bone microstructure, showing therapeutic effects similar to the commercial drug PERIOCLINE® (PERIO). Furthermore, LIRA@PLGA/HA reduced the expression of necroptosis-related factors RIPK1, RIPK3, and MLKL. In conclusion, these results suggest that topical application of LIRA@PLGA/HA is effective for the treatment of DP through inhibition of necroptosis, representing a promising treatment strategy.

1. Introduction

Periodontitis and diabetes are among the most prevalent chronic inflammatory diseases globally. As of 2021, there were approximately 529 million patients with diabetes worldwide, and it is estimated that this number will rise to 1.31 billion by 2050 [1]. According to the WHO data for 2022, severe periodontal disease affects over 1 billion individuals aged 15 and older worldwide [2]. These two conditions are closely related and exhibit bidirectional correlation [3,4]. Toxins, metabolites, and inflammatory factors produced by periodontal pathogens can induce systemic inflammation via the oral-gut or periodontal pocket-blood pathways, stimulating the release of inflammatory factors in patients with diabetes [5]. This contributes to the onset of insulin resistance and alterations in glucose metabolism [6], thereby affecting blood glucose control. Conversely, diabetes can modulate host responses to periodontal pathogens through advanced glycation end products (AGEs), adipokines, cytokines, bone metabolism, and immune responses, thereby influencing the progression of periodontitis [7,8].

* Corresponding author. School/Hospital of Stomatology, Lanzhou University, Lanzhou, Gansu, 730000, China.wangjing@lzu.edu.cn
E-mail addresses: pangyunqing@126.com (Y. Pang), kongly21@lzu.edu.cn (L. Kong), liyuanyuan3784@163.com (Y. Li), 2458498311@qq.com (J. Li), maql18@lzu.edu.cn (Q. Ma), 2637454305@qq.com (J. Qiu).
[1] These authors contributed equally.

https://doi.org/10.1016/j.mtbio.2025.101582
Received 15 August 2024; Received in revised form 12 January 2025; Accepted 14 February 2025
Available online 15 February 2025

Studies have found that the prevalence of periodontitis is 57.9 % in diabetic populations compared to 15.0 % in non-diabetic populations [9]. Diabetes and periodontitis show mutual exacerbation, posing significant challenges for treating periodontitis in a diabetic microenvironment.

Currently, treatment for diabetes-related periodontitis primarily involves multiple short-term non-surgical periodontal therapies under the premise of glycemic control, including mechanical plaque removal and adjunctive drug therapy [10]. However, these treatments often fail to achieve completely satisfactory results. The latest clinical practice guidelines developed by the European Federation of Periodontology suggest considering the topical application of antimicrobials and antibiotics as adjuncts to subgingival devices for the treatment of stage I-III periodontitis [11]. The American Dental Association's clinical practice guidelines even recommend the use of doxycycline hyclate gel and minocycline microspheres as "expert opinion" for adjunctive therapy [12]. While this does not mean that we endorse this recommendation [13], it underscores the importance of the use of topical antimicrobial agents in the treatment of DP. However, the use of antimicrobial agents is inevitably associated with potential side effects and the development of resistant bacteria [14]. Research by Rams et al. [15] found that approximately 74.2 % of subgingival plaques are resistant to one or more tested antibiotics. Researchers have focused on the use of anti-diabetic medications and found that metformin, glucagon-like peptide-1 (GLP-1) receptor agonists, and sulfonylureas have therapeutic effects on periodontitis [16–19]. Our previous research showed that the hypoglycemic agent liraglutide (LIRA), when administered systemically, not only reduces blood sugar but also reduces inflammatory infiltration of periodontal tissue caused by periodontitis and reduces alveolar bone loss in diabetic rats, thereby potentially treating diabetes-related periodontitis [20]. However, systemic administration of LIRA has drawbacks, including short duration of action, low topical effective concentration, and significant side effects. Therefore, it is necessary to design a rational strategy for the topical administration of LIRA to maintain effective drug concentrations in the periodontal microenvironment.

Poly (lactic-co-glycolic acid) (PLGA) is a synthetic copolymer composed of lactic acid and glycolic acid monomers, known for its excellent biocompatibility and biodegradability. It has been approved by the United States Food and Drug Administration (US FDA) and the European Medicines Agency (EMA) for various medical applications [21]. Bydureon®, a sustained-release formulation of exenatide-4 using PLGA as a carrier, demonstrates prolonged drug release for several weeks, significantly extending the duration of action of exenatide-4 *in vivo* [22]. Shi et al. [23] developed microspheres loaded with exenatide-4 using PLGA and chitosan to improve impaired implant osseointegration in diabetes. The microspheres containing 0.2 % (w/v) of chitosan demonstrated an encapsulation efficiency of 53.97 ± 1.78 %, a drug loading capacity of 0.14 ± 0.01 %, and exhibited stable, slow drug release over approximately 30 days, indicating their excellent performance as a drug delivery system. Pereira et al. [24] prepared metformin-PLGA nanoparticles for treating periodontitis in diabetic rats, demonstrating that the PLGA nanoparticles could enhance the efficacy of metformin hydrochloride, control its release, and prolong its action *in vivo*. In summary, PLGA holds broad prospects in drug delivery and sustained release and offers flexible control over the duration of drug release through adjustment of the preparation parameters [25].

Therefore, this study aimed to prepare PLGA particles loaded with LIRA (LIRA@PLGA) and encapsulated in natural hyaluronic acid (HA) hydrogel, constructing a LIRA-loaded periodontal sustained-release system (LIRA@PLGA/HA). The study investigated the therapeutic effects and potential mechanisms of this system on periodontitis in diabetic rats and used minocycline ointment PERIOCLINE® (PERIO) as a positive control, providing a new method for clinically treating diabetes-related periodontitis.

2. Materials and methods

2.1. Synthesis of LIRA@PLGA/HA

PLGA nanoparticles were synthesized using a modified emulsion solvent evaporation technique. Initially, 5 mg of lyophilized LIRA (Novo Nordisk, Hillerød, Denmark) was dissolved in 0.1 mL of triple-distilled water (pH = 8), forming the inner aqueous phase. Concurrently, 100 mg of PLGA (carboxyl-terminated with lactide/glycolide ratio 50/50, Daigangbiao, Jinan, China) was dissolved in 1 mL of dichloromethane, creating the oil phase. The aqueous phase was gradually introduced into the oil phase via syringe, forming an oil-in-water (O/W) emulsion through ultrasonication in an ice bath. The theoretical maximum drug loading was 5 %. Subsequently, this emulsion was rapidly injected into an outer aqueous phase (pH = 5.5) containing 1 % polyvinyl alcohol (PVA) as an emulsifier and sonicated for 5 min in the same ice bath, resulting in a water-in-oil-in-water (W/O/W) complex emulsion. The organic solvent dichloromethane was then evaporated by magnetic stirring at low speed for 4–6 h under a fume hood. Finally, the nanoparticles were collected via high-speed centrifugation at 12 000 rpm for 10 min, washed three times with triple-distilled water, and freeze-dried to obtain LIRA@PLGA nanoparticles. Furthermore, 5 mg of lyophilized LIRA@PLGA was dispersed in 1 mL of triple-distilled water. Then, add 15 mg of HA to create a hydrogel (LIRA@PLGA/HA).

2.2. Characterization of LIRA@PLGA/HA

The microstructure of PLGA nanoparticles was examined using scanning electron microscopy (SEM, JEOL, JSM6701F, Japan). PLGA nanoparticle suspension droplets were applied to silicon wafers for natural air drying then sputter coating them with gold prior to imaging. Coating was performed at 4 mA for 10 min. Particle size and distribution coefficient were determined by dynamic light scattering (DLS). Drug binding to nanoparticles was analyzed by Fourier-transform infrared spectroscopy (FTIR, Bruker, USA), while circular dichroism (CD) spectroscopy assessed the conformational stability of LIRA within the nanoparticles. The inner and outer aqueous phases were labeled with sodium fluorescein, and the structure of LIRA@PLGA was observed by Laser scanning confocal microscope.

The high performance liquid chromatography (HPLC) technique was employed to detect LIRA. The original LIRA solution was prepared to achieve a mass concentration of 20 mg/L. The HPLC method facilitated the determination of the drug peak time under specific conditions: the mobile phase consisted of an acetonitrile-water solution in a volume ratio of 60:40; the detection wavelength was set at 215 nm; the column temperature was maintained at 35 °C; the flow rate was established at 1 ml/min, and an injection volume of 20 μl was utilized.

To prepare a stock solution, precisely measure 0.6 mg of LIRA into a 5 mL centrifuge tube, then add an appropriate amount of PBS and mix thoroughly to obtain a stock solution with a concentration of 320 mg/L. This stock solution was subsequently diluted by factors of two to generate standard solutions with concentrations of 160, 80, 40, 20, 10, and 5 mg/L. Under the aforementioned HPLC conditions, these solutions were analyzed for determination. A plot depicting peak area (Y) against corresponding concentration (X) will be constructed to assess linearity and establish the standard curve (Fig. S6).

For drug encapsulation analysis, 10 mg of drug-loaded PLGA nanoparticles were ultrasonically dissolved in 1 mL of dichloromethane, extracted with 1 mL PBS (pH = 8), transferred of water-soluble drugs to PBS and centrifuged at 8000 rpm. The aqueous phase was collected and the process repeated thrice. The supernatants were pooled, and the drug concentration determined by HPLC. Drug loading and encapsulation efficiency were calculated as follows:

$$Drug\ loading\ (\%) = \frac{Amount\ of\ drug\ estimated\ in\ nanoparticle}{Amount\ of\ nanoparticle} \times 100$$

$$Encapsulation\ efficiency\ (\%) = \frac{Drug\ loading}{Theoretical\ maximum\ drug\ loading} \times 100$$

The drug-loaded PLGA nanoparticles were suspended in a closed container with 4 mL of PBS. The suspension was then oscillated at 50 rpm in a thermostatic oscillator set at 37 °C. Samples were collected at time points of 12, 24, 48, 72, 96, 120, 144, 168, and 192 h respectively. Drug concentrations were determined by HPLC at each time point and drug release curves were plotted. All experiments were conducted with three parallel groups.

2.3. Biocompatibility of LIRA@PLGA/HA

Human periodontal ligament cells (HPDLCs) were obtained from primary culture. Human tooth samples were used for primary culture and obtained from two consenting donors with ethical approval from the School of Stomatology, Lanzhou University. The Cell Counting Kit-8 (CCK-8) assay assessed the effect of LIRA@PLGA/HA on HPDLCs viability to determine cytotoxicity. HPDLCs were cultured in 96-well plates at a density of 5×10^3 cells/well for 24 h. Cells were then treated with LIRA@PLGA/HA gels containing different LIRA@PLGA concentrations (1.25, 2.5, 5, 10, 20 mg/mL) for 24 h. Subsequently, 10 μl of CCK-8 solution (5 g/L, Sigma, St. Louis, MO, USA) was added per well and incubated at 37 °C for 2 h. Absorbance was measured at 450 nm using an enzyme marker (Tecan, Switzerland).

2.4. Establishment of an experimental model of diabetes-associated periodontitis

Male Wistar rats (90–110g, n = 60) were randomly divided into 2 groups: diabetic group (n = 48) and non-diabetic group (n = 12). Then, the non-diabetic rats were randomly divided into 2 groups: normal control group (Normal, n = 6) and periodontitis group (P, n = 6). The animals were acclimatized for 1 week under clean conditions with a 12 h light/dark cycle, at 24–26 °C and 60%–75 % humidity. The diabetic group received a high-fat diet (HFD, 65 % basal diet, 10 % lard, 20 % sucrose, 2.5 % cholesterol, and 1 % sodium cholate) for 1 month. Diabetes was induced with a low dose of streptozotocin (STZ, 35 mg/kg), and rats with fasting blood glucose (FBG) > 11.1 mmol/L for 3 consecutive days were considered diabetic. However, 9 rats were died during the establishment of the diabetic rat models. The diabetic rats (n = 39) were randomly assigned to groups: diabetic (DM, n = 7), DP (DP + NaCl, n = 8), DP + blank system (DP + PLGA/HA, n = 8), DP + PERIO (Sunstar, Osaka, Japan, n = 8), and DP + LIRA@PLGA/HA (n = 8). Periodontitis was induced by ligating 4-0 cotton thread around the maxillary second molar for 4 weeks. Drugs (200 μl) were injected into the gingival sulcus around the left maxillary second molars once a week for four weeks. The periodontal-related clinical indicators, including the gingival bleeding index (BI), probing depth (PD), and tooth movement (TM), were measured.

Animal care and experiments were conducted in accordance with the protocol approved by the Ethical Research Committee of Lanzhou University School of Stomatology (LZUKQ-2020-014) and were approved by "Guidelines for Animal Care and Use" (NIH).

2.5. Oral glucose tolerance test (OGTT)

After a 12 h fast, oral glucose (2 g/kg body weight) was administered via gavage. Blood glucose levels were measured using the Accu-Chek active system (Roche, Germany) at 0, 60, 90, 120, and 180 min post-administration via tail vein blood samples.

2.6. Histological evaluation

Fresh left maxillary and gingival tissues were fixed in 4 % paraformaldehyde for 24–48 h. Tissues were rinsed with deionized water and decalcified in 10 % EDTA for 6 weeks, with weekly changes of the decalcification solution. Post-decalcification, tissues were dehydrated, embedded, and sectioned (5 μm thick) along the mesiodistal axis of the second molar. H&E staining assessed inflammation in rat periodontal tissues. And the alveolar bone was stained with methylene blue to observe the resorption of alveolar bone.

2.7. Enzyme-linked immunosorbent assay (ELISA)

Prior to collecting gingival sulcus fluid, soft tartar and plaque were removed from the left maxillary second molar using wet cotton swabs, and the tooth surface was dried with sterile cotton balls. Moisture-absorbent paper was gently inserted into the periodontal pocket for 30 s and then placed into an EP tube containing 150 μL PBS. This process was repeated three times with 1 min intervals. After elution for 1 h, 100 μL of supernatant was centrifuged at 1500 rpm for 5 min and stored at −80 °C. Whole blood was collected via cardiac puncture, stored at room temperature for 2 h, centrifuged at 1000 rpm for 15 min, and the supernatant used for analysis. ELISA kits (Multi Sciences, China) measured TNF-α and IL-1β protein levels, expressed in picograms/milliliter, with triplicate measurements averaged.

2.8. Micro-CT

The left maxillary specimens were obtained post-euthanasia, fixed in 4 % paraformaldehyde for 24 h, and transferred to 70 % ethanol for CT scanning (SkyScan 1176; Bruker, Germany). Horizontal alveolar bone loss was measured from the cemento-enamel junction to the alveolar bone crest along the long axis of the second molar roots. Furthermore, the images of alveolar bone around the left maxillary second molar was selected as the region of interest (ROI), and the following parameters were analyzed included bone mineral density (BMD), bone volume fraction (BV/TV), trabecular number (Tb.N), trabecular thickness (Tb. Th), and trabecular separation (Tb.Sp).

2.9. Quantitative real-time reverse transcriptase PCR (qRT-PCR)

Total RNA from gingival tissue was extracted using TRIzol reagent (Invitrogen, Carlsbad, CA, USA), and mRNA was reverse-transcribed using the RT reagent kit (Takara, Japan). qRT-PCR was performed using SSoAdvanced SYBR Green Supermix. Primer sequences were.

- **RIPK-1**: forward 5′-GCCACTTAAGCCCAAGTGCAG-3′, reverse 5′-TCATCCCGGCAGTGCTCTATC-3′
- **RIPK-3**: forward 5′-TACTGCACCGGGACCTCAAG-3′, reverse 5′-GTGGACAGGCCAAAGTCTGCTA-3′
- **MLKL**: forward 5′-TCTGTGCTTAGAGACATGGGCATAC-3′, reverse 5′-GCCATACAGAGCATCCAGCAA
- **β-actin**: forward 5′-TCAGGTCATCACTATCGGCAAT-3′, reverse 5′-AAAGAAAGGGTGTAAAACGCA

2.10. Western blot analysis

Western blot analysis involved scraping tissues in RIPA lysis buffer (50 mM Tris-HCl, pH 7.4, 2 mM EDTA, 2 % SDS) supplemented with protease inhibitors (Roche, China). Protein samples were resolved by 10 % SDS-PAGE and transferred to PVDF membranes using a semi-dry transfer apparatus. Antibodies used were anti-receptor-interacting protein kinase 1 (RIPK-1) (Immuno Way, Plano, TX, USA), anti-receptor-interacting protein kinase 3 (RIPK-3) (Abcam, Cambridge, MA, USA), mixed lineage kinase domain-like protein (MLKL) (Immuno Way, Plano, TX, USA), and β-actin (Immuno Way, Plano, TX, USA). Protein bands were detected using ECL detection reagents.

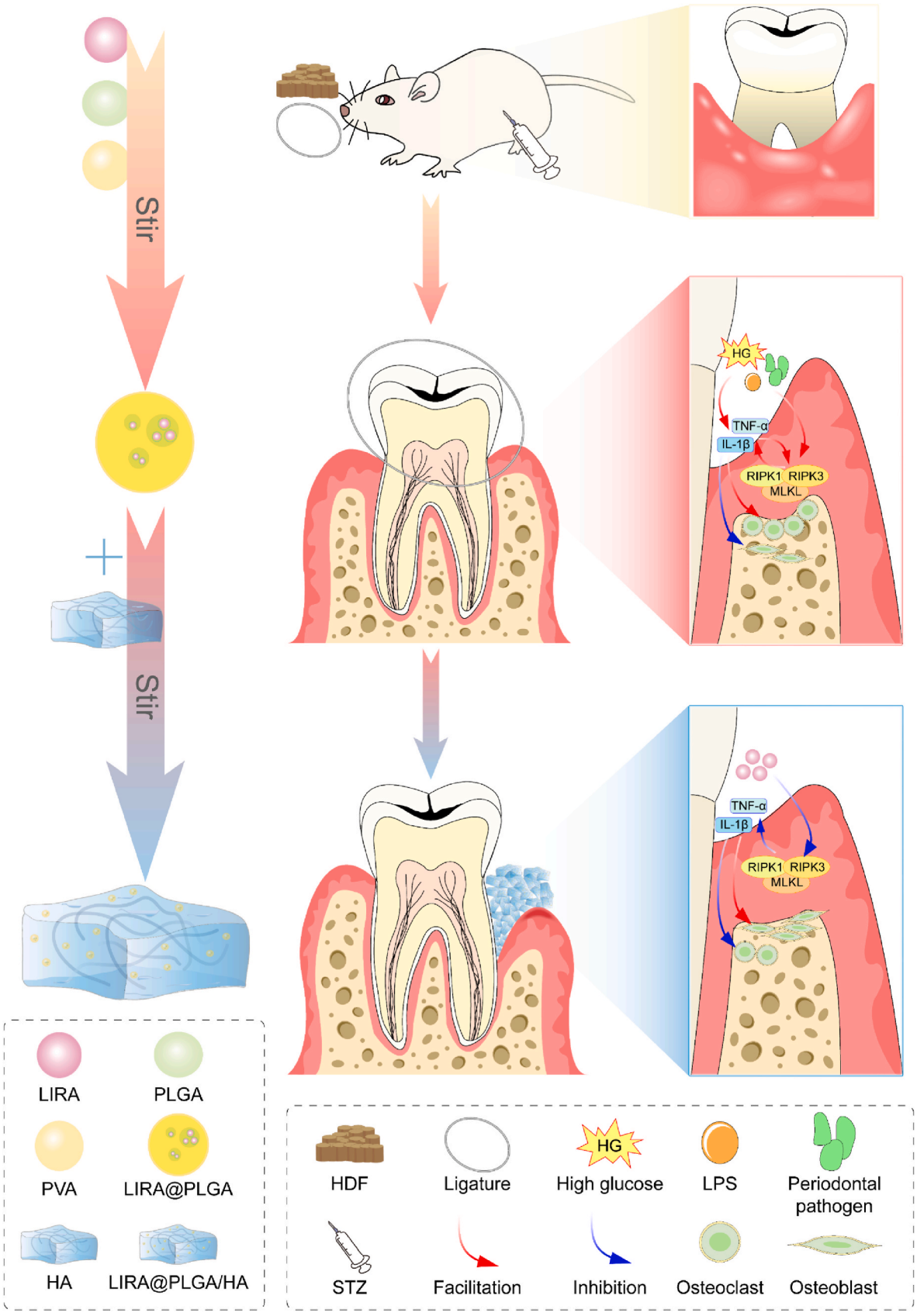

Fig. 1. Schematic illustration of the LIRA@PLGA/HA sustained-release system for treating periodontitis in diabetic rats, demonstrating its role in modulating necroptosis. Significantly increased levels of the inflammatory factors TNF-α and IL-1β were observed in the periodontal microenvironment of DP rats, along with increased expression of necroptosis-related molecules RIPK1, RIPK3, and MLKL. Treatment with the LIRA@PLGA/HA sustained-release system reduced the levels of inflammatory factors and necroptosis-related molecules and promoted alveolar bone regeneration. This suggests that LIRA@PLGA/HA can achieve sustained release of LIRA in periodontal tissues and treat DP by inhibiting necroptosis.

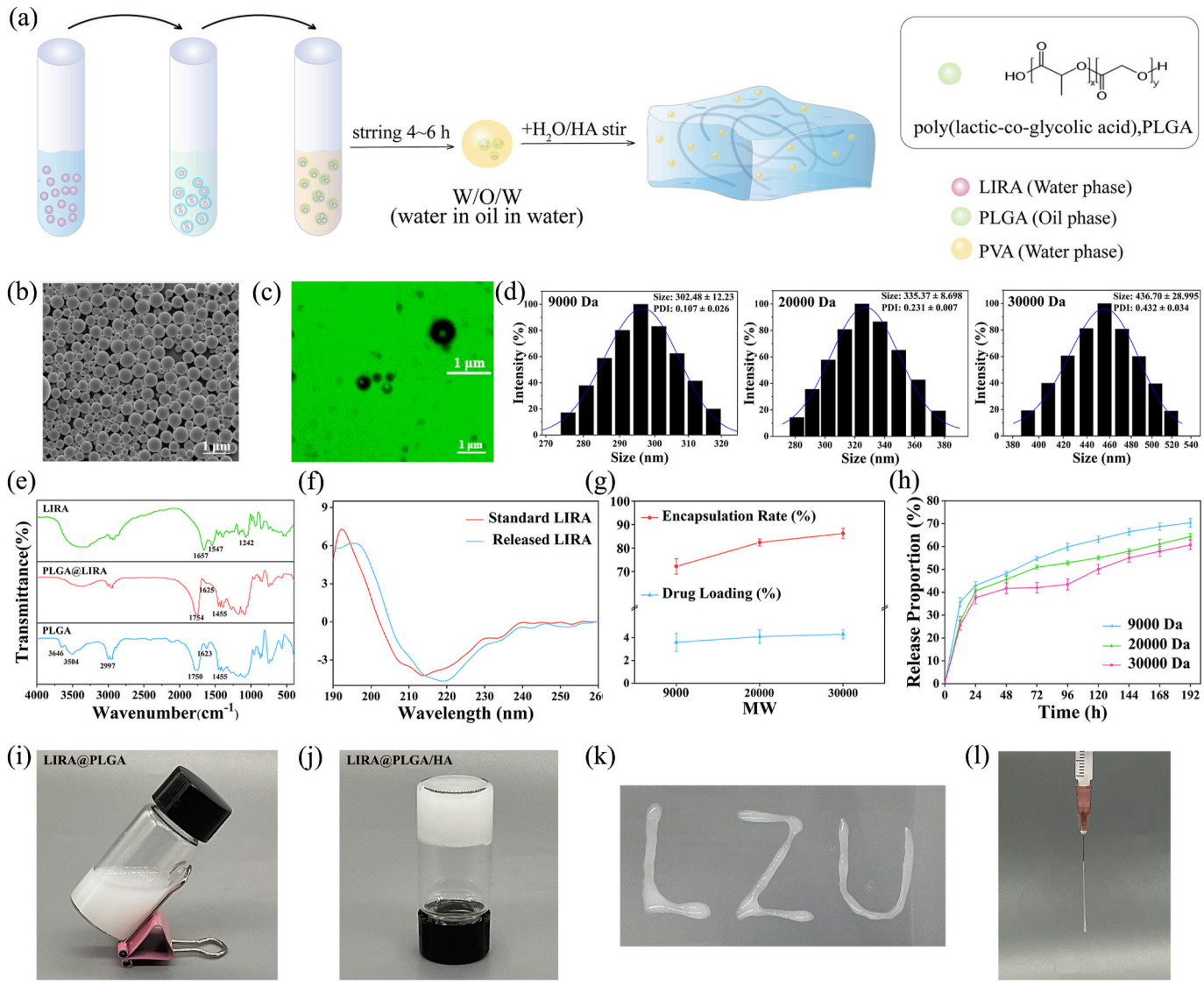

Fig. 2. Synthesis and characterization of LIRA@PLGA. (a) Schematic diagram of LIRA@PLGA/HA synthesis; (b) Scanning electron microscopy image of PLGA nanoparticles; (c) Laser scanning confocal microscope image of LIRA@PLGA nanoparticles; (d) Size and distribution of LIRA@PLGA nanoparticles with different molecular weights; (e) FTIR spectra of LIRA, PLGA, and LIRA@PLGA nanoparticles; (f) Circular dichroism spectra of LIRA standard solution and released LIRA from PLGA nanoparticles; (g) Encapsulation efficiency and drug loading of LIRA@PLGA nanoparticles; (h) Drug release curves of LIRA@PLGA nanoparticles; (i) The photograph of LIRA@PLGA dispersed in water; (j) The photograph of LIRA@PLGA/HA after gelatinization; (k, l) Photographs of the letters of "LZU", which were written by extruding the LIRA@PLGA/HA through a needle.

2.11. Statistical analysis

Statistical analyses were conducted using SPSS (Chicago, IL, USA). Data are presented as mean ± standard deviation (SD). Statistical comparisons were performed using one-way ANOVA, with P values < 0.05 considered statistically significant (see Fig. 1).

3. Results and discussion

3.1. Synthesis, characterization, and biosafety of the LIRA@PLGA/HA sustained-release system

PLGA drug-loaded nanoparticles have broad applications in drug encapsulation and are often prepared using emulsion solvent evaporation methods [26,27]. This study chose a modified emulsion evaporation method (re-emulsion method) to synthesize LIRA@PLGA nanoparticles. This method is suitable for encapsulating peptides or protein drugs, requiring the use of double emulsification to form W/O/W multiple emulsions (Fig. 2a). SEM results showed that the PLGA nanoparticles were spherical, and the particle size ranged essentially from 200 to 500 nm (Fig. 2b). The inner and outer aqueous phases were labeled with sodium fluorescein, and a typical W/O/W structure was observed in LIRA@PLGA nanoparticles by Laser scanning confocal microscope (Fig. 2c). FTIR spectroscopy was used to analyze the interaction between LIRA and the PLGA nanoparticles during synthesis (Fig. 2e). The characteristic spectrum of PLGA included peaks near 3523-3654 cm^{-1} related to OH stretching, peaks near 2884-3000 cm^{-1} related to stretching vibrations of CH, CH_2, and CH_3, a peak near 1750 cm^{-1} related to ester bonds, and peaks near 846-1459 cm^{-1} related to (C-H) bending. The LIRA spectrum showed characteristic peaks at 1657, 1547, and 1242 cm^{-1}, attributed to bending vibrations of amines I (-NH_2), amines II (-NH-), and amines III (C-N). The spectrum of LIRA@PLGA did not differ significantly from that of the blank PLGA, with the characteristic LIRA peaks assigned to amides masked by the PLGA peaks, consistent with previous reports [28] and demonstrating the encapsulation of LIRA in nanoparticles. The biological efficacy of LIRA depends

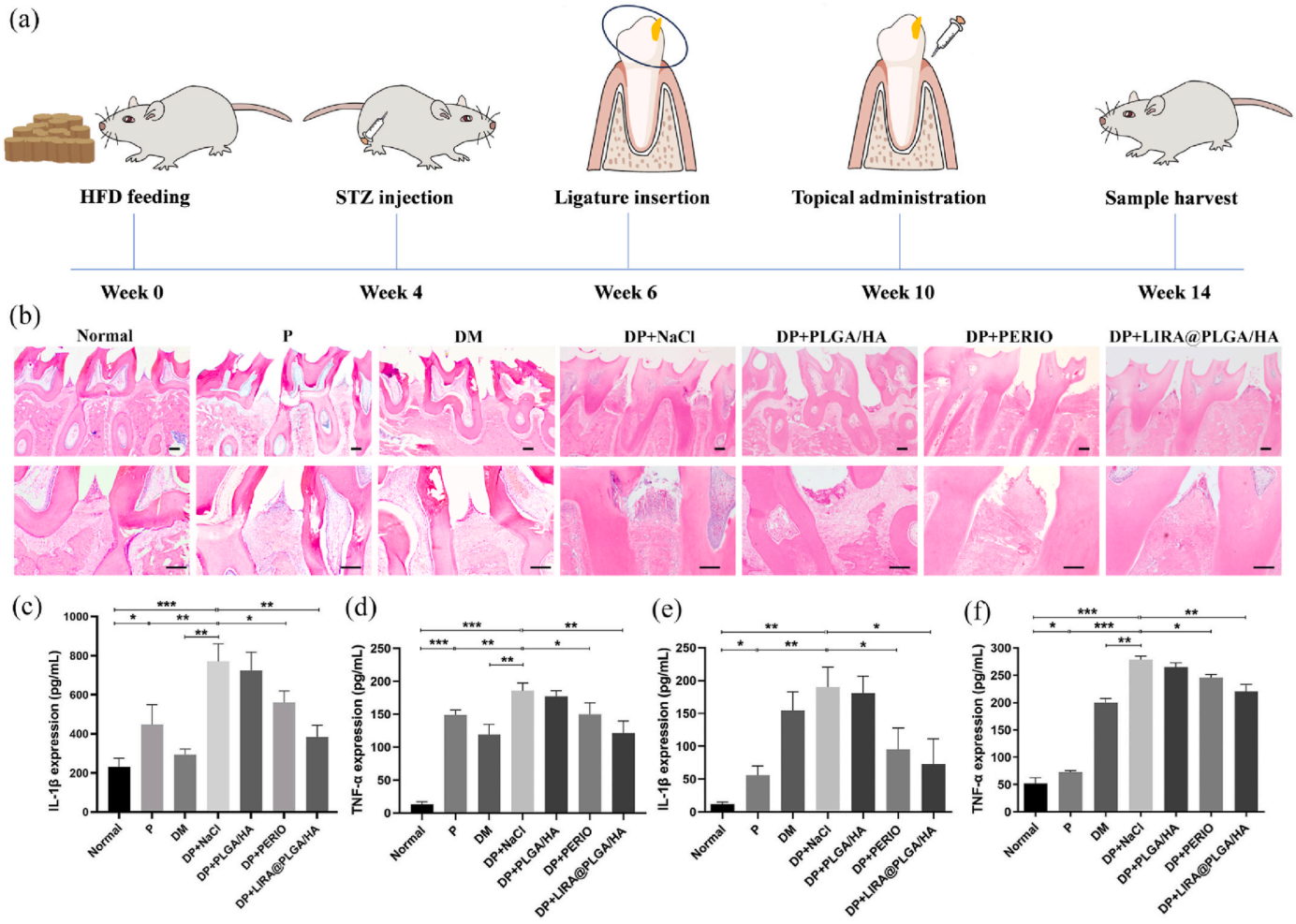

Fig. 3. Anti-inflammatory effect of LIRA@PLGA/HA on DP. (a) Timeline showing establishment of the DP rat model; (b) H&E staining of periodontal tissues, scale bar = 200 μm; (c), (d) Expression of IL-1β and TNF-α in the serum; (e), (f) Expression of IL-1β and TNF-α in the gingival crevicular fluid. *$P < 0.05$, **$P < 0.01$, ***$P < 0.001$.

on the integrity of its secondary structure; thus, CD spectroscopy was used to assess the conformational stability of LIRA released from PLGA nanoparticles (Fig. 2f). The results showed that the CD spectrum of the LIRA standard solution showed positive values at 190 nm in the far-ultraviolet region, and negative values at 208 nm and 222 nm, indicating the presence of an α-helical structure, consistent with previous studies on the typical structure of GLP-1 [29]. Moreover, LIRA released from PLGA nanoparticles showed no significant changes in conformation, with unchanged peak intensities (the α-helical structure content was unchanged), demonstrating that the secondary structure of LIRA was not altered during the encapsulation process.

The molecular weight of PLGA affects the particle size, drug loading, encapsulation efficiency, and final drug-release profile of the drug-loaded nanoparticles. In this study, three different molecular weights of PLGA (9000, 20 000, and 30 000 Da) were chosen for the synthesis of the LIRA@PLGA nanoparticles. The results showed that the average particle sizes of the LIRA@PLGA nanoparticles were 302.48 ± 12.23 nm, 335.37 ± 8.698 nm and 436.70 ± 28.995 nm, respectively, and correlated positively with the molecular weight of PLGA (Fig. 2d). Correspondingly, the polydispersity index (PDI) were 0.107 ± 0.026, 0.231 ± 0.007 and 0.432 ± 0.034, respectively (Fig. 2d). The results of PDI showed that the LIRA@PLGA became highly polydisperse and broadening their particle size distribution with the increase of molecular weight. The three types of PLGA nanoparticles exhibited over 70 % encapsulation efficiency (72.2 %, 82.4 % and 86.2 %, respectively) and over 3.5 % drug loading (3.6 %, 4.1 % and 4.3 %, respectively), with the higher molecular-weight particles showing greater drug loading and encapsulation efficiencies (Fig. 2g). The drug release from all three LIRA@PLGA nanoparticles reached approximately 25 % within 12 h, meeting the high-concentration drug environment at the initial stage of administration. Over the following 8 days, LIRA was slowly and continuously released from the nanoparticles, with the cumulative release reaching about 60 % after 8 days (Fig. 2h), indicating that the prepared LIRA@PLGA nanoparticles met the requirement for sustained release. Furthermore, the drug-release curves indicated that the initial burst of release from the higher molecular-weight PLGA nanoparticles was lower, together with slower release rates (Fig. 2h), consistent with previous research results [30]. Therefore, considering that LIRA@PLGA nanoparticles synthesized with 30000 Da PLGA exhibited the highest encapsulation efficiency and drug loading, as well as a relatively reduced release at the initial burst, they were selected for subsequent synthesis of drug-loaded nanoparticles. Additionally, the selection of PLGA also focused end-capping. Researchers have reported that end-capped PLGA exhibits higher encapsulation efficiency compared to uncapped PLGA, attributed to its stronger polarity [31]. The present study chose carboxyl-terminated PLGA, where the carboxyl group facilitates binding with peptide amino groups.

Low molecular weight HA is known to promote both proliferation and osteogenic differentiation in human mesenchymal stem cells [32, 33]. Therefore, to ensure optimal topical action of LIRA@PLGA

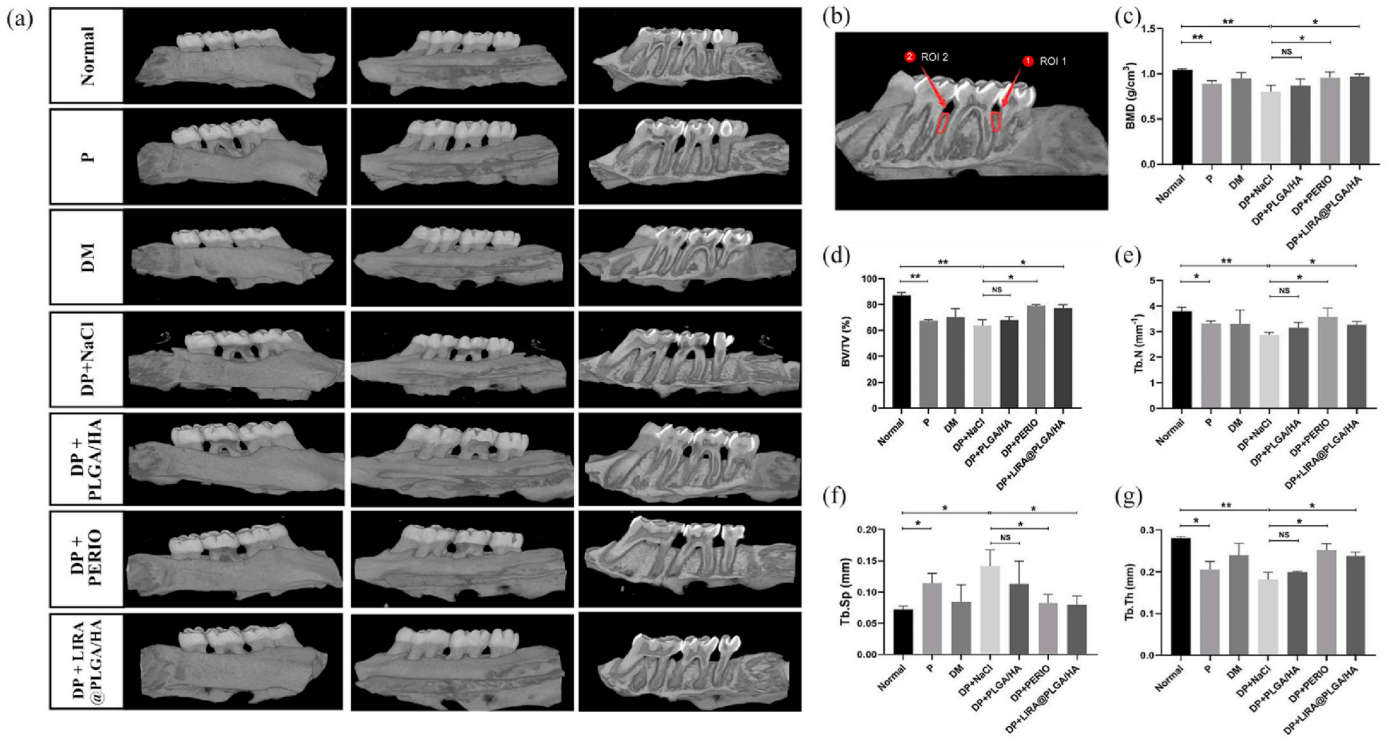

Fig. 4. Effect of LIRA@PLGA/HA on alveolar bone in diabetic rats. (a) Representative micro-CT images of the left maxilla obtained by 3D reconstruction; (b) ROI marked for subsequent analysis; (c) Quantitative analysis of bone density; (d) Quantitative analysis of bone volume/total volume; (e), (f) Quantitative analysis of trabecular thickness; (g) Quantitative analysis of trabecular separation. *$P < 0.05$, **$P < 0.01$.

nanoparticles on periodontal tissues, a low molecular-weight (90–100 kDa) HA hydrogel was used to encapsulate and disperse the LIRA@PLGA nanoparticles, creating a LIRA@PLGA/HA sustained-release system. As shown in Fig. 2i–j, the addition of HA (15 mg/ml) to the LIRA@PLGA aqueous solution resulted in a stable gel state. To evaluate the injectability of the LIRA@PLGA/HA hydrogel, we filled it into a syringe system and labeled it "LZU" for injection purposes (Fig. 2k–l). The findings demonstrated that the LIRA@PLGA/HA hydrogel exhibited excellent injectability, facilitating convenient filling of irregular periodontal pockets. Despite the biosafety demonstrated by PLGA and HA, it was essential to evaluate the cytotoxicity of the LIRA@PLGA/HA system. The potential toxicity of different concentrations (1.25, 2.5, 5, 10, 20 mg/mL LIRA@PLGA) of LIRA@PLGA/HA on HPDLCs was thus assessed using CCK-8 assays. The results indicated that after 24 h of stimulation with various concentrations of LIRA@PLGA/HA, cell viability remained above 85 % (Fig. S1), demonstrating the favorable biosafety of LIRA@PLGA/HA.

3.2. Anti-inflammatory effects of LIRA@PLGA/HA on DP

An experimental rat model of DP was established using HFD + low-dose STZ (35 mg/kg) injection, and cotton ligature around the maxillary second molars (Fig. 3a). The results of OGTT showed that the abnormal glucose tolerance in DM group (Fig. S2), which confirmed that a stable model of diabetes was established using HFD+35 mg/kg STZ (single intraperitoneal injection). This is similar to previous studies [34,35]. Despite the relative safety of low-dose STZ, deaths occurred during the model establishment, possibly due to three reasons: STZ's cytotoxicity to multiple organs [36,37]; hypoglycemia within 24 h post-injection (complete insulin release from destroyed pancreatic islet cells), which is a high-risk period for death, followed by gradual blood glucose elevation [38]; accidental injection of STZ into the sub-peritoneal space [34,35]. In summary, HFD+35 mg/kg STZ injection is recommended for establishing diabetic rat models, with precautions such as fasting before surgery and glucose supplementation after surgery to prevent hypoglycemia-related deaths.

Ligation for the induction of periodontitis remains the classic method [39,40]. We used a 4-0 non-absorbable surgical suture around the rat's second molars, which promotes microbial accumulation due to the suture's roughness. Additionally, a small amount of high-sugar high-fat diet was fed to enhance the adhesion of food to the tooth surfaces, disrupting oral self-cleaning, and effectively simulating periodontitis progression. Four weeks after ligation, compared to normal control and diabetic rats, the rats in the DP group and P group exhibited gingival redness (Figs. S3a–d), severe bleeding on probing (Fig. S3e), the formation of periodontal pockets (Fig. S3f), and loosening of teeth (Fig. S3g). Moreover, compared to the P group, the periodontal condition was worse in the rats in the DP group. Histological staining of the rat maxillae with methylene blue revealed significant absorption of alveolar bone in the DP and P groups, compared to the normal group, with more severe alveolar bone destruction observed in the DP group (Figs. S3h and i). These findings confirmed the successful establishment of the rat DP model.

The treatment of DP still focuses on the control of inflammation. After topical treatment with LIRA@PLGA/HA for 4 weeks, clinical periodontal indicators (BI and PD) were reassessed. The results showed that these indicators were significantly decreased in the DP + LIRA@PLGA/HA and DP + PERIO groups compared to the DP group, whereas no significant difference was seen with the DP + PLGA/HA group (Figs. S4b and c). Histological sections of the maxillary second molars stained with hematoxylin and eosin (H&E) showed that compared to the normal group, rats in the DP + NaCl group showed evident migration of the gingival epithelium toward the root, alveolar bone absorption, and infiltration of inflammatory cells in the intrasulcular epithelium. After drug treatment, the inflammation was significantly reduced in the DP + PERIO and DP + LIRA@PLGA/HA groups, while the DP + PLGA/HA and DP + NaCl groups showed no significant differences in inflammation compared to those before

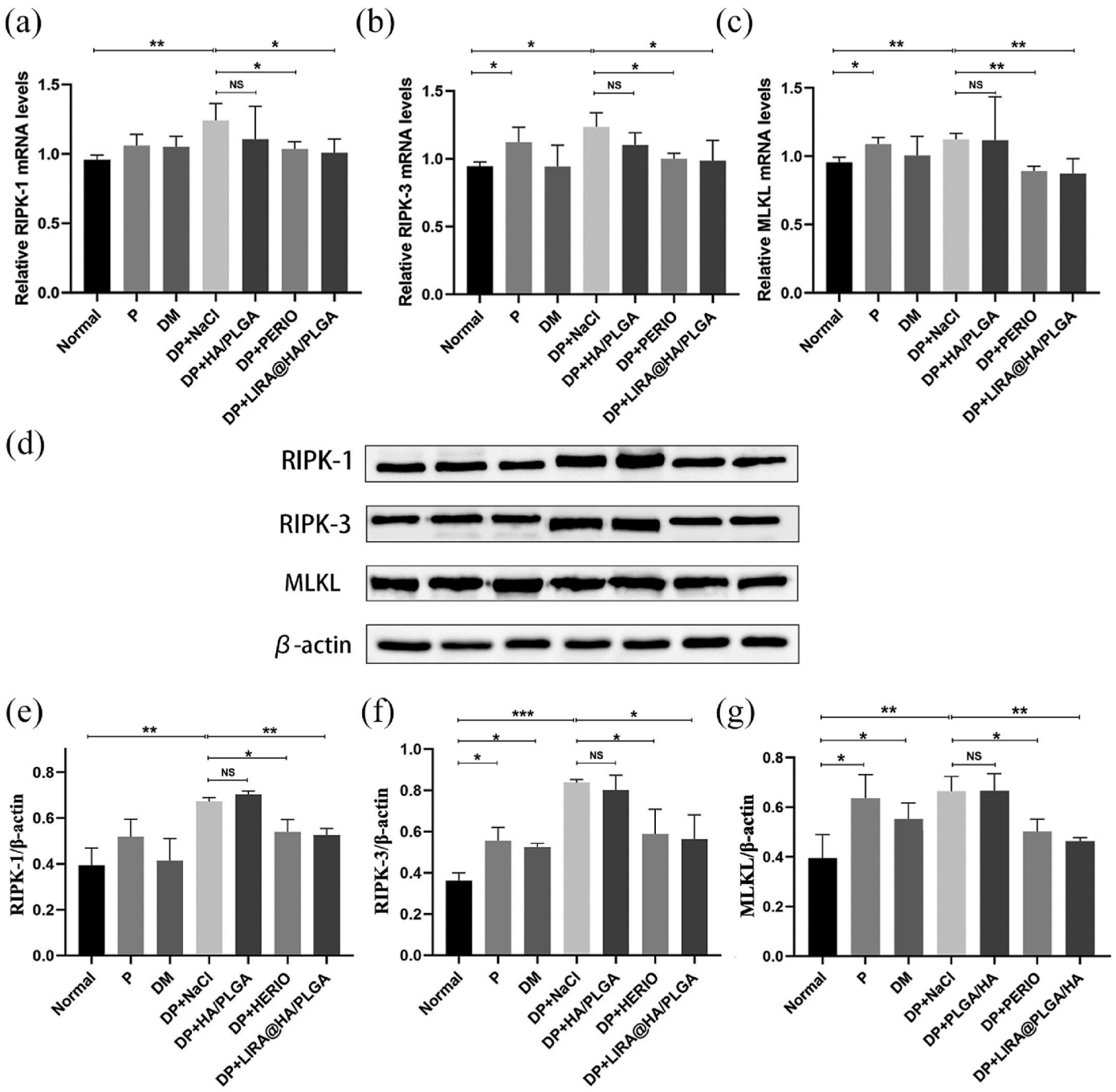

Fig. 5. Effects of LIRA@PLGA/HA on necroptosis. (a–c) The mRNA expression of RIPK-1, RIPK-1 and MLKL in gingival tissue of rats; (d–g) The protein expression of RIPK-1, RIPK-1 and MLKL in gingival tissue of rats. *$P < 0.05$, **$P < 0.01$, ***$P < 0.001$.

treatment (Fig. 3b). The expression of inflammatory factors in blood and gingival sulcus fluid of the maxillary second molars was measured by ELISA. Compared to the normal group, the expression of the inflammatory factors TNF-α and IL-1β in the blood and gingival crevicular fluid of rats in the P group, diabetes mellitus (DM) group, and DP + NaCl group was markedly increased, with the DP + NaCl group showing the most significant increase (Fig. 3c–f), further confirming successful establishment and maintenance of the rat DP model. After topical drug treatment, TNF-α and IL-1β expression in serum and gingival crevicular fluid of the rats in the DP + LIRA@PLGA/HA and DP + PERIO groups was significantly reduced compared to that in the DP + NaCl group, while no significant differences were seen between the DP + PLGA/HA and DP + NaCl groups (Fig. 3c–f). These results suggested that PLGA/HA had no therapeutic effect on DP inflammation but did not exacerbate it, demonstrating favorable biosafety, while topical treatment with LIRA@PLGA/HA significantly inhibited inflammatory reactions in DP, showing a therapeutic effect similar to that of the positive control (PERIO). Interestingly, there were changes in the serum levels of inflammatory factors after topical administration, likely due to improvement in inflamed periodontal pocket walls, preventing bacteria and toxic factors from entering the bloodstream, which offered some experimental basis for periodontal treatment to improve the management of DM. Evidence-based medicine also suggests that periodontal intervention effectively reduces serum inflammatory factor expression in patients with DM and chronic periodontitis [41,42].

3.3. Protective effect of LIRA@PLGA/HA on alveolar bone in DP

To further observe the effects on bone tissue post-administration, macroscopic observations and micro-CT scans of the alveolar bone were performed. Compared to the normal group, there was no significant absorption of alveolar bone in the DM group, while noticeable absorption was observed in the P and DP groups, with the DP group showing more severe destruction, including buccolingual-penetrating root bifurcation lesions (Fig. 4a). The topical drug treatment significantly reduced alveolar bone loss compared to the DP + NaCl group (Fig. 4a). Micro-CT was used to convert the ROI near the maxillary second molars into three-dimensional volumes of interest (VOI) for quantitative analysis of the bone microstructure. The results showed that compared to the DP + NaCl group, parameters such as BMD, BV/TV, Tb.Th, and Tb.N in the LIRA@PLGA/HA and PERIO treatment groups were increased, while Tb.Sp showed the opposite trend (Fig. 4b–g), consistent with the macroscopic observations (Fig. S5). The therapeutic effects of LIRA@PLGA/HA are consistent with the results of our previous studies involving systemic administration of LIRA [20], demonstrating the feasibility of LIRA for topical periodontal treatment. Importantly, topical application significantly reduced the dose of LIRA (168 μg per rat, Table S1). From this point of view, the topical application of LIRA has more advantages in the treatment of diabetic periodontitis.

3.4. LIRA@PLGA/HA May improve periodontitis by inhibiting necroptosis

Inflammation is a common feature of diabetes and periodontitis and is a key target for the treatment of DP. Necroptosis is associated with various inflammatory diseases, including periodontitis and diabetes [43–46]. Necroptosis is a caspase-independent form of cell death that is activated to prevent blocked apoptosis [47,48]. Necroptosis is mediated by necrosomes, which consist of MLKL, RIPK1, and RIPK3 [48,49]. Shi et al. [50] found that the gingivae of patients with untreated chronic periodontitis contained elevated levels of RIPK1, p-RIPK3, MLKL, and p-MLKL, and necroptosis mediated by these proteins was involved in the pathogenesis of periodontitis. Another study [51] found that compared to patients with periodontitis, those with diabetes-associated periodontitis had higher gingival levels of RIPK1, RIPK3, and p-MLKL proteins. Significantly, LIRA may play a protective role in liver by reducing the expression of RIPK1, RIPK3 and MLKL [52]. Therefore, it is speculated that LIRA may exert anti-inflammatory effects by inhibiting necroptosis, thereby alleviating periodontal disease.

The impact of LIRA@PLGA/HA on the expression of necroptosis-related factors was analyzed by qRT-PCR and Western blotting. The results showed that the mRNA and protein levels of RIPK1, RIPK3, and MLKL in the DP + NaCl group were significantly higher than those in the normal group, which are consistent with the present findings [51]. After treatment with LIRA@PLGA/HA or PERIO, the expression levels of RIPK1, RIPK3, and MLKL mRNA and protein were significantly reduced ($P < 0.05$), whereas HA/PLGA treatment had no significant effect on RIPK1, RIPK3, and MLKL expression (Fig. 5). These results suggested that LIRA@PLGA/HA may exert a therapeutic effect on periodontitis by inhibiting necroptosis, similar to the effects of the clinical medication PERIO. Notably, PERIO exhibited inhibitory effects on necroptosis-related pathways, warranting further investigation.

4. Conclusion

In this study, LIRA@PLGA nanoparticles were successfully synthesized by re-emulsion method, presenting W/O/W structure, which showed excellent release capability without affecting the efficacy of LIRA. Furthermore, low molecular weight HA was used to develop a LIRA@PLGA/HA hydrogel sustained-release system, which exhibited favorable gelatinization properties and injectability. The topical application of this hydrogel significantly alleviated inflammation in diabetic rats with periodontitis, reduced alveolar bone loss, and improved bone tissue formation, which exhibited therapeutic effects similar to commercial minocycline ointment PERIO. Additionally, LIRA@PLGA/HA may exert therapeutic effects by inhibiting necroptosis, providing further theoretical support for LIRA as a potential clinical adjunctive drug for the treatment of DP.

CRediT authorship contribution statement

Yunqing Pang: Writing – review & editing, Writing – original draft, Methodology, Conceptualization. **Lingyuan Kong:** Writing – original draft, Software, Resources. **Yuanyuan Li:** Methodology, Investigation, Data curation. **Jiamin Li:** Software, Formal analysis, Data curation. **Qianlong Ma:** Resources, Methodology, Formal analysis. **Jing Qiu:** Software, Methodology, Formal analysis. **Jing Wang:** Writing – review & editing, Validation, Funding acquisition, Conceptualization.

Declaration of competing interest

The authors declare the following financial interests/personal relationships which may be considered as potential competing interests: Jing Wang reports financial support was provided by the Scientific and Technological Foundation of Gansu Province. If there are other authors, they declare that they have no known competing financial interests or personal relationships that could have appeared to influence the work reported in this paper.

Acknowledgments

This study was supported by the Scientific and Technological Foundation of Gansu Province (20YF8FA073, 20JR10FA670), and the School/Hospital of Stomatology Lanzhou University (lzukqky-2022-t09).

Appendix A. Supplementary data

Supplementary data to this article can be found online at https://doi.org/10.1016/j.mtbio.2025.101582.

Data availability

Data will be made available on request.

References

[1] K.L. Ong, L.K. Stafford, S.A. Mclaughlin, et al., Global, regional, and national burden of diabetes from 1990 to 2021, with projections of prevalence to 2050: a systematic analysis for the Global Burden of Disease Study 2021, Lancet 402 (10397) (2023) 203–234.
[2] WHO, Global Oral Health Status Report—Towards Universal Health Coverage for Oral Health by 2030, World Health Organization, Geneva, 2022.
[3] C.-Z. Wu, Y.-H. Yuan, H.-H. Liu, et al., Epidemiologic relationship between periodontitis and type 2 diabetes mellitus, BMC Oral Health 20 (1) (2020).
[4] N. Shi, C. Kong, L. Yuan, et al., The bidirectional relationship between periodontitis and diabetes: new prospects for stem cell-derived exosomes, Biomed. Pharmacother. (2023) 165.
[5] L.X.X. Lili, W. Yun, et al., Advances in research on the mechanism of association between periodontitis and diabetes mellitus, J. Sichuan Univ. 54 (1) (2023) 71–76.
[6] R. Komazaki, S. Katagiri, H. Takahashi, et al., Periodontal pathogenic bacteria, Aggregatibacter actinomycetemcomitans affect non-alcoholic fatty liver disease by altering gut microbiota and glucose metabolism, Sci. Rep. 7 (1) (2017).
[7] J. StöHR, J. Barbaresko, M. Neuenschwander, et al., Bidirectional association between periodontal disease and diabetes mellitus: a systematic review and meta-analysis of cohort studies, Sci. Rep. 11 (1) (2021).
[8] H. Qin, G. Li, X. Xu, et al., The role of oral microbiome in periodontitis under diabetes mellitus, J. Oral Microbiol. 14 (1) (2022).
[9] A. Popławska-Kita, K. Siewko, P. Szpak, et al., Association between type 1 diabetes and periodontal health, Adv. Med. Sci. 59 (1) (2014) 126–131.
[10] T. Kocher, J. KöNIG, W.S. Borgnakke, et al., Periodontal complications of hyperglycemia/diabetes mellitus: Epidemiologic complexity and clinical challenge, Periodontology 78 (1) (2000) 59–97, 2018.

[11] C.J. Smiley, S.L. Tracy, E. Abt, et al., Evidence-based clinical practice guideline on the nonsurgical treatment of chronic periodontitis by means of scaling and root planing with or without adjuncts, J. Am. Dent. Assoc. 146 (7) (2015) 525–535.
[12] O.L. Tan, S.H. Safii, M. Razali, Clinical efficacy of repeated applications of local drug delivery and adjunctive agents in nonsurgical periodontal therapy: a systematic review, Antibiotics 10 (10) (2021).
[13] N. West, I. Chapple, N. Claydon, et al., BSP implementation of European S3 - level evidence-based treatment guidelines for stage I-III periodontitis in UK clinical practice, J. Dent. (2021) 106.
[14] A. Arredondo, V. Blanc, C. Mor, et al., Resistance to β-lactams and distribution of β-lactam resistance genes in subgingival microbiota from Spanish patients with periodontitis, Clin. Oral Invest. 24 (12) (2020) 4639–4648.
[15] T.E. Rams, J.E. Degener, A.J. Van Winkelhoff, Antibiotic resistance in human chronic periodontitis microbiota, J. Periodontol. 85 (1) (2014) 160–169.
[16] V.C.M. Neves, L. Satie Okajima, E. Elbahtety, et al., Repurposing Metformin for periodontal disease management as a form of oral-systemic preventive medicine, J. Transl. Med. 21 (1) (2023).
[17] Y. Zhang, X. Yuan, Y. Wu, et al., Liraglutide regulates bone destruction and exhibits anti-inflammatory effects in periodontitis in vitro and in vivo, J. Dent. 94 (2020).
[18] M. Wang, M. Liu, J. Zheng, et al., Exendin-4 regulates the MAPK and WNT signaling pathways to alleviate the osteogenic inhibition of periodontal ligament stem cells in a high glucose environment, Open Med. 18 (1) (2023).
[19] L. Yang, Q. Ge, Z. Ye, et al., Sulfonylureas for treatment of periodontitis-diabetes comorbidity-related complications: killing two birds with one stone, Front. Pharmacol. 12 (2021).
[20] M. Yang, Y. Pang, M. Pei, et al., Therapeutic potential of liraglutide for diabetes–periodontitis comorbidity: killing two birds with one stone, J. Diabetes Res. 2022 (2022) 1–10.
[21] Y. Su, B. Zhang, R. Sun, et al., PLGA-based biodegradable microspheres in drug delivery: recent advances in research and application, Drug Deliv. 28 (1) (2021) 1397–1418.
[22] T. Li, A. Chandrashekar, A. Beig, et al., Characterization of attributes and in vitro performance of exenatide-loaded PLGA long-acting release microspheres, Eur. J. Pharm. Biopharm. 158 (2021) 401–409.
[23] S. Shi, S. Song, X. Liu, et al., Construction and performance of exendin-4-loaded chitosan–PLGA microspheres for enhancing implant osseointegration in type 2 diabetic rats, Drug Deliv. 29 (1) (2022) 548–560.
[24] A.D.S.B.F. Pereira, G.A.D.C. Brito, M.L.D.S. Lima, et al., Metformin hydrochloride-loaded PLGA nanoparticle in periodontal disease experimental model using diabetic rats, Int. J. Mol. Sci. 19 (11) (2018).
[25] Y. Xu, C.S. Kim, D.M. Saylor, et al., Polymer degradation and drug delivery in PLGA-based drug–polymer applications: a review of experiments and theories, J. Biomed. Mater. Res. B Appl. Biomater. 105 (6) (2016) 1692–1716.
[26] L. Wang, P. Wang, Y. Liu, et al., The effect of different factors on poly(lactic-co-glycolic acid) nanoparticle properties and drug release behaviors when Co-loaded with hydrophilic and hydrophobic drugs, Polymers 16 (7) (2024).
[27] Y. Hua, Y. Su, H. Zhang, et al., Poly(lactic-co-glycolic acid) microsphere production based on quality by design: a review, Drug Deliv. 28 (1) (2021) 1342–1355.
[28] S.I. Elsayed, G.N.S. Girgis, M.S. El-Dahan, Formulation and evaluation of pravastatin sodium-loaded PLGA nanoparticles: in vitro–in vivo studies assessment, Int. J. Nanomed. 18 (2023) 721–742.
[29] R. Ismail, T. SováNY, A. GáCSI, et al., Synthesis and statistical optimization of poly (lactic-Co-glycolic acid) nanoparticles encapsulating GLP1 analog designed for oral delivery, Pharm. Res. 36 (7) (2019).
[30] M. Ochi, B. Wan, Q. Bao, et al., Influence of PLGA molecular weight distribution on leuprolide release from microspheres, Int. J. Pharm. 599 (2021).
[31] M.A.J. Blanco-PrıETO, M.A. Campanero, K. Besseghir, et al., Importance of single or blended polymer types for controlled in vitro release and plasma levels of a somatostatin analogue entrapped in PLA/PLGA microspheres, J. Contr. Release 96 (3) (2004) 437–448.
[32] B. Teng, S. Zhang, J. Pan, et al., A chondrogenesis induction system based on a functionalized hyaluronic acid hydrogel sequentially promoting hMSC proliferation, condensation, differentiation, and matrix deposition, Acta Biomater. 122 (2021) 145–159.
[33] E. Chiesa, A. Greco, F. Riva, et al., CD44-Targeted carriers: the role of molecular weight of hyaluronic acid in the uptake of hyaluronic acid-based nanoparticles, Pharmaceuticals 15 (1) (2022).
[34] S.N. Goyal, N.M. Reddy, K.R. Patil, et al., Challenges and issues with streptozotocin-induced diabetes – a clinically relevant animal model to understand the diabetes pathogenesis and evaluate therapeutics, Chem. Biol. Interact. 244 (2016) 49–63.
[35] J. Wang, Y. He, D. Yu, et al., Perilla oil regulates intestinal microbiota and alleviates insulin resistance through the PI3K/AKT signaling pathway in type-2 diabetic KKAy mice, Food Chem. Toxicol. (2020) 135.
[36] E. Pirabbasi, M.M. Zangeneh, A. Zangeneh, et al., Chemical characterization and effect of Ziziphora clinopodioides green-synthesized silver nanoparticles on cytotoxicity, antioxidant, and antidiabetic activities in streptozotocin-induced hepatotoxicity in Wistar diabetic male rats, Food Sci. Nutr. 12 (5) (2024) 3443–3451.
[37] M.A.S. Di Leo, S.A. Santini, S.N. Gentiloni, et al., Long-term taurine supplementation reduces mortality rate in streptozotocin-induced diabetic rats, Amino Acids 27 (2) (2004) 187–191.
[38] A.J.S. Ghasemi, Streptozotocin as a tool for induction of rat models of diabetes: a practical guide, Excli j 22 (2023) 274–294.
[39] D.C. Tomina, Ş.A. Petruțiu, C.M. Dinu, et al., Comparative testing of two ligature-induced periodontitis models in rats: a clinical, histological and biochemical study, Biology 11 (5) (2022).
[40] Y.-H. Wu, Y. Taya, R. Kuraji, et al., Dynamic microstructural changes in alveolar bone in ligature-induced experimental periodontitis, Odontology 108 (3) (2019) 339–349.
[41] W.Y.Z. Miaomiao, W. Chong, et al., Influence of periodontal non-surgical therapy on serum interleukin 6 expression and carotid artery wall in rats with periodontitis and type 2 diabetes mellitus, West China J. Stomatol. 37 (6) (2019) 589–593.
[42] A.S.K.M. Aziz, A. Suryakar, et al., Pre-and post-treatment effectiveness of SRP on levels of IL-6, IL-10, and CRP in chronic periodontitis patients with and without diabetes, Am. J. Biochem. 8 (1) (2018) 1–6.
[43] X. Hua, B. Li, F. Yu, et al., Protective effect of MFG-E8 on necroptosis-induced intestinal inflammation and enteroendocrine cell function in diabetes, Nutrients 14 (3) (2022).
[44] H. Pang, G. Huang, Z. Xie, et al., The role of regulated necrosis in diabetes and its complications, J. Mol. Med. 102 (4) (2024) 495–505.
[45] Y. Yang, L. Wang, H. Zhang, et al., Mixed lineage kinase domain-like pseudokinase-mediated necroptosis aggravates periodontitis progression, J. Mol. Med. 100 (1) (2021) 77–86.
[46] K. Zhang, X. Chen, R. Zhou, et al., Inhibition of gingival fibroblast necroptosis mediated by RIPK3/MLKL attenuates periodontitis, J. Clin. Periodontol. 50 (9) (2023) 1264–1279.
[47] J. Seo, Y.W. Nam, S. Kim, et al., Necroptosis molecular mechanisms: recent findings regarding novel necroptosis regulators, Exp. Mol. Med. 53 (6) (2021) 1007–1017.
[48] K. Newton, A. Strasser, N. Kayagaki, et al., Cell death, Cell 187 (2) (2024) 235–256.
[49] K. Ye, Z. Chen, Y. Xu, The double-edged functions of necroptosis, Cell Death Dis. 14 (2) (2023).
[50] J. Shi, J. Li, W. Su, et al., Loss of periodontal ligament fibroblasts by RIPK3-MLKL-mediated necroptosis in the progress of chronic periodontitis, Sci. Rep. 9 (1) (2019).
[51] L. Ou, T. Sun, Y. Cheng, et al., MicroRNA-214 contributes to regulation of necroptosis via targeting ATF4 in diabetes-associated periodontitis, J. Cell. Biochem. 120 (9) (2019) 14791–14803.
[52] M.M. Atef, N.A. Abou Hashish, Y.M. Hafez, et al., The potential protective effect of liraglutide on valproic acid induced liver injury in rats: targeting HMGB1/RAGE axis and RIPK3/MLKL mediated necroptosis, Cell Biochem. Funct. 41 (8) (2023) 1209–1219.